SUPPORTING INFORMATION
for
Observation of Haldane Magnetism in Organically Templated Vanadium Phosphate $(enH_2)_{0.5}VPO_4OH$

A.Sh. Samarin,[1] S.S. Fedotov,[1] H.-J. Koo,[2] M.-H. Whangbo,[2,3] A.A. Gippius,[4,5] S.V. Zhurenko,[5] A.V. Tkachev,[5] L.V. Shvanskaya,[4,6] A.N. Vasiliev[4,6]

[1]Skolkovo Institute of Science and Technology, Moscow 121205, Russia
[2]Kyung Hee University, Seoul 02447, Republic of Korea
[3]North Carolina State University, Raleigh, North Carolina 27695-8204, USA
[4]Lomonosov Moscow State University, Moscow 119991, Russia
[5]Lebedev Physical Institute, RAS, Moscow 119991, Russia
[6]National University of Science and Technology, Moscow 119049, Russia

Synthesis and X-ray diffraction

Table S1. Chemicals used for the synthesis in deionized H_2O (5 μS cm^{-1}; Membrane-based deionizer)

Chemical	Purity, other notes	Supplier
Vanadium oxide (III) V_2O_3	99.7% metals basis	Alfa Aesar
Phosphoric acid H_3PO_4 (85 mass. % solution in H_2O)	ACS reagent, reducing substances, passes test ≤0.001% volatile acids (as CH_3COOH)	Sigma Aldrich
Ethylenediamine $H_2N(CH_2)_2NH_2$	99%	Ruskhim LLC

Table S2. Atomic coordinates and thermal parameters for $(enH_2)_{0.5}VPO_4OH$ from Rietveld refinement

Atom	Wyckoff	*x/a*	*y/b*	*z/c*
V1	4*e*	0.0100(12)	0.1557(10)	0.2492(4)
P1	4*e*	-0.5094(13)	-0.0934(19)	0.1515(4)
O1	4*e*	0.149(4)	0.401(4)	0.1940(1)
O2	4*e*	-0.318(3)	0.109(3)	0.1727(8)
O3	4*e*	-0.743(3)	-0.119(3)	0.2112(9)
O4	4*e*	-0.324(4)	-0.303(3)	0.1641(9)
O5	4*e*	-0.674(2)	-0.091(3)	0.0769(6)
N1	4*e*	-1.061(4)	0.233(4)	0.0446(10)
C1	4*e*	-1.100(6)	-0.412(8)	0.0130(13)
H1	4*e*	-1.21(3)	0.19(4)	0.020(8)
H2	4*e*	-1.24(4)	-0.47(4)	0.05(1)

H3	4*e*	-1.18(6)	-0.35(4)	0.03(1)
H4	4*e*	-1.14(3)	0.27(3)	0.084(7)
H5	*4e*	-0.93(3)	0.12(3)	0.05(1)
H6	*4e*	0.31(4)	0.36(4)	0.180(9)

Bond lengths for the O-H (O1–H6 bond), N-H, C–H were fixed in the range 0.83-0.87 Å, 0.85-0.95 Å and 1.45-1.55 Å based on Refs. [1-3].

Comparison of $(enH_2)_{0.5}VPO_4OH$ and NH_4VPO_4OH crystal structures

The new compound, $(enH_2)_{0.5}VPO_4OH$, relates structurally to the previously described phase, NH_4VPO_4OH, but they are not isostructural. The first phase crystallizes in the $P2_1/c$ space group, while the second phase in the $P2_1/m$ space group. A comparative analysis of their crystal structures reveals similar two-dimensional structural fragments. These sheets are built up from the chains of edge-sharing VO_5OH octahedra strengthened by the PO_4 tetrahedra. The V-O chains run along the *b* axis in both crystal structures, as shown in the Fig. S1. The resulting V-P-O sheets are perpendicular to the *a* and *c* axes in NH_4VPO_4OH and $(enH_2)_{0.5}VPO_4OH$, respectively. In NH_4VPO_4OH, 2_1-axes pass through vanadium atoms, so neighboring V-P-O sheets are connected by simple translation. In the crystal structure of $(enH_2)_{0.5}VPO_4OH$, the 2_1-axes link symmetrically the neighboring V-P-O fragments, leading to a doubling of the *c*-axis compared to the *a*-axis of NH_4VPO_4OH, as shown in Fig. S1. This difference is due to the arrangement of larger ethylenediamine molecules in the interlayer space, compared to more compact ammonium groups.

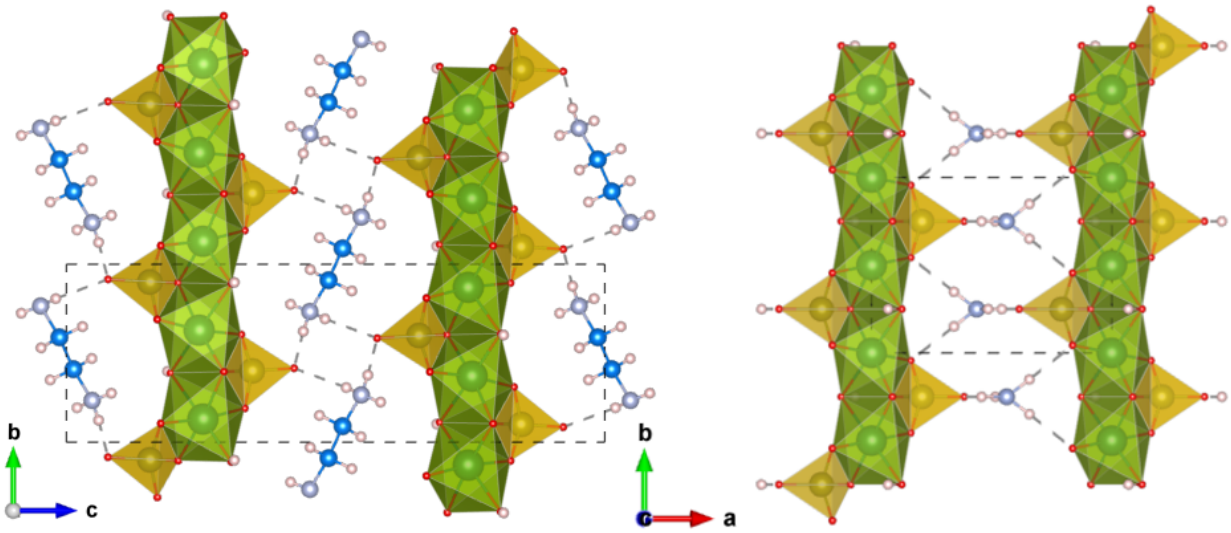

Fig. S1. Structurally related crystal structures of $(enH_2)_{0.5}VPO_4OH$ (left) and NH_4VPO_4OH (right), which are based on the 2D fragments of chains of edge-sharing VO_5OH octahedra strengthened by the PO_4 tetrahedra. V – light green, P – yellow, O – red, N – light blue, C – intense blue, H – pale pink.

Nuclear magnetic resonance

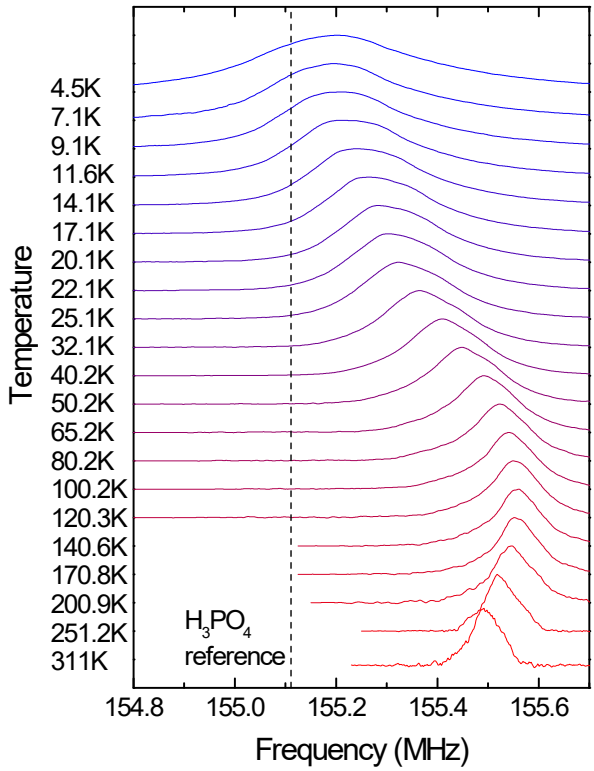

Figure S2. Evolution with temperature of the ^{31}P NMR spectra obtained at $\mu_0 H = 9$ T.

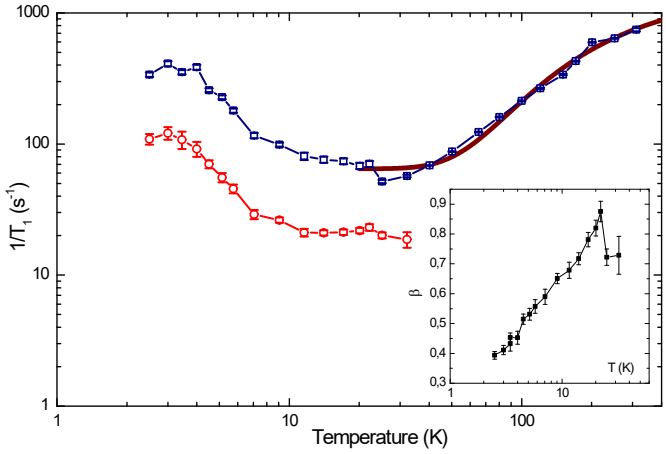

Figure S3. Temperature dependences of the fast and slow ^{31}P spin-lattice relaxation rates in $(enH_2)_{0.5}VPO_4OH$ measured at 9 T. Fast relaxation component is depicted by blue squares, with the slow component by red circles. Inset: stretching factor β of the slow relaxing component as a function of temperature.

As discussed in the main text, we attribute the fast-relaxing component $1/T_{1\text{fast}}$ of nuclear spin-lattice relaxation (NSLR) curves to the relaxation through the $S = 1$ spins of the Haldane chains. Above the spin-glass formation broad maximum, it would be reasonable to observe Haldane-like temperature behavior. In general, the NSLR rate due to magnetic centers can be written as [4]:

$$1/T_1 = 2\gamma_n^2 k_B T \sum_q |A(q)|^2 \frac{\chi''(q,\omega_n)}{\omega_n},$$

where γ_n is the nuclear gyromagnetic ratio, $A(q)$ is the hyperfine coupling, and $\chi''(q, \omega_n)$ is the dissipative component of the dynamic susceptibility evaluated at the nuclear Larmor frequency ω_n and wave vector q.

Indeed, the data in the range of 20 – 311 K can be described by an activation law with an additional constant term $1/T_{1fast} = 1/T_{1const} + A^*\exp(-\Delta_R/k_BT)$ (the thick line on the **Fig. S3**), typical of gapped magnetic systems. The retrieved relaxation gap $\Delta_R = 229\pm18$ K is much higher than the value from the line shift data. However, the overestimation of the spin gap value in the NSLR experiments is common for Haldane systems; it arises at least from the dynamic susceptibility, involved in the relaxation process, as well as $A(q)$, while $K(T)$ and $\chi(T)$ deal only with the static one at $q = 0$ [5]. Various studies indicate different values for the relationship $\gamma = \Delta_R/\Delta$ between the relaxation gap Δ_R and the conventional gap $\Delta = 0.41J$ [3]. One of the most widely accepted value for γ is 1.5 [6-9]. Some theoretical studies estimate γ as 2 [10,11], and Pahari *et al*. even used the values of $3 = 1.5\times2$ [12]. However, even this approach leads to a slightly higher gap of 229/3 K = 76 K (compared with 48.4 K obtained from ^{31}P NMR shift data). Some additional discrepancy may appear since most estimates of Δ_R are made for relatively low temperatures $k_BT < \Delta$, which can only be partially used in our case due to the spin-glass contribution. Nevertheless, it is important to note the observation of a spin gap also from the NSLR data.

The stretching factor β starts to decrease below 20 K, indicating an increase in the degree of disorder in the system (see the inset of Fig.S3). This result correlates with the increase in $1/T_1$ below 10 K and provides an additional piece of evidence for the emergence of a disordered spin glass state at temperatures around 3 K.

Density functional theory. Supplementary discussion

A. Spin exchanges J_1 and J_2 of $(en H_2)_{0.5}VPO_4OH$ and NH_4VPO_4OH

To evaluate the spin exchanges of **$(enH_2)_{0.5}VPO_4OH$ and NH_4VPO_4OH** using the energy-mapping analyisi [13-15], we carry out DFT+U calculations for the (a, 2b, c) supercell of $(enH_2)_{0.5}VPO_4OH$ and NH_4VPO_4OH using the frozen core projector augmented plane wave (PAW) [16] encoded in the Vienna ab Initio Simulation Packages (VASP) [17] and the PBE potential [18] for the exchange-correlation functional. The electron correlation associated with the 3*d* states of Co was taken into consideration by DFT+U calculations with an effective on-site repulsion $U_{eff} = U - J = 2$ and 3 eV [19].

(1) Spin exchange paths

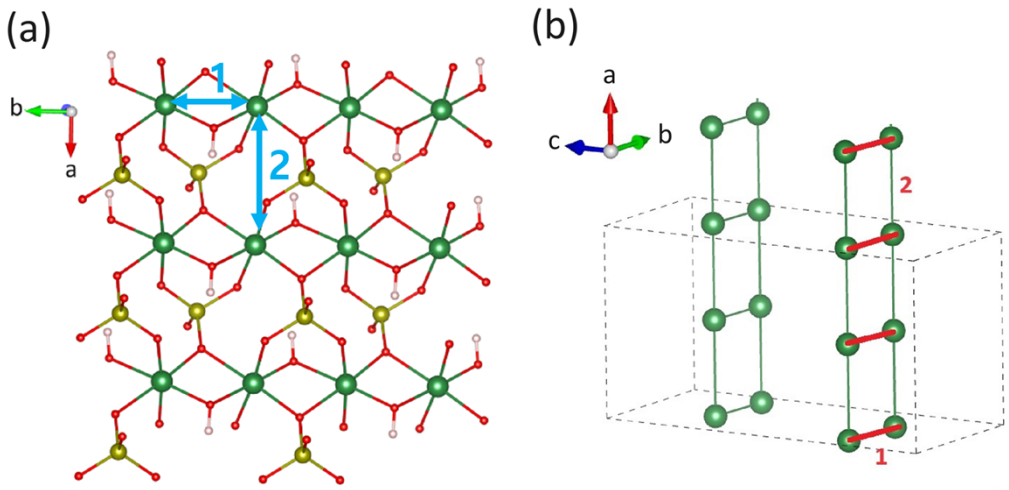

Figure S4. (a) A single VPO_4OH layer of $(enH_2)_{0.5}VPO_4OH$ showing how the edge-sharing ribbon chains are interconnected by the PO_4 groups to form a VPO_4OH layer, where the labels 1 and 2 refer to the intrachain and interchain spin exchange paths J_1 and J_2, respectively. (b) Arrangement of the spin exchange paths J_1 and J_2 in $(enH_2)_{0.5}VPO_4OH$.

NOTE: The spin arrangement of ***Fig. S4b*** *is also valid for* NH_4VPO_4OH.

(2) Three ordered spin states used for the mapping analysis

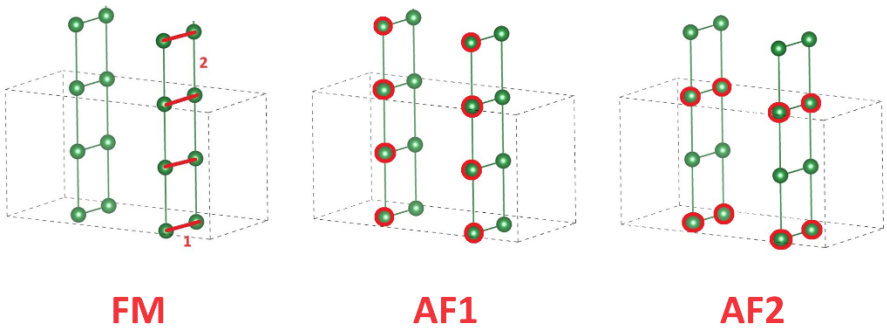

Figure S5. Spin arrangements of the ordered spin states FM, AF1, and AF2, where the green spheres without and with red circles represent up-spin and down-spin Co^{2+} ion sites, respectively.

(3) Energies of the ordered spin states in terms of the spin exchanges

$$E_{FM} = (-8J_1 - 8J_2)S^2$$
$$E_{AF1} = (+8J_1 - 8J_2)S^2$$
$$E_{AF2} = (-8J_1 + 8J_2)S^2$$

(4) Spin exchanges in terms of the energies of the ordered spin states

$$J_1 = (E_{AF1} - E_{FM})/(16S^2)$$
$$J_2 = (E_{AF2} - E_{AF1})/(16S^2)$$

(5) Relative energies of the ordered spin states in terms of DFT+U calculations

a) Computational parameters

Exchange-correlation functional: PBE
Threshold for SCF convergence: 10^{-6} eV
k-point: (6x8x2) for $(enH_2)_{0.5}VPO_4OH$
(8x10x8) for NH_4VPO_4OH
Plane wave cut-off energy: 450 eV

b) Results

Table S3. Relative energies (in meV/f.u.) obtained from DFT+U calculations

For $(enH_2)_{0.5}VPO_4OH$

	U_{eff} = 2 eV	U_{eff} = 3 eV
FM	25.31	20.91
AF1	0	0
AF2	25.37	20.85

For NH_4VPO_4OH

	U_{eff} = 2 eV	U_{eff} = 3 eV
FM	16.00	12.58
AF1	0	0
AF2	15.44	12.06

(6) Values of the spin exchanges

The values of J_1 and J_2 determined by the energy-mapping analyses are summarized in the main text.

B. Single-ion anisotropy of $(enH_2)_{0.5}VPO_4OH$ and NH_4VPO_4O

(1) Local Cartesian coordinates

To estimate the single-ion anisotropy of the V^{3+} ions in $(enH_2)_{0.5}VPO_4OH$ and NH_4VPO_4O, we first replace all but one V^{3+} ions of a unit cell with nonmagnetic ions Ga^{3+} to obtaina hypothetical structure that has one VO_6 octahedron containing a V^{3+} ion in a unit cell. Then we carry out DFT+U+SOC calculations [20] for this hypothetical structure using the local Cartesian coordinate defined for the VO_6 octahedron as defined in **Figure S6**, where we choose the local z-axis of the VO_6 octahedron along the shortest V-O bond (hereafter, the ||z direction), and the ⊥z direction perpendicular to it.

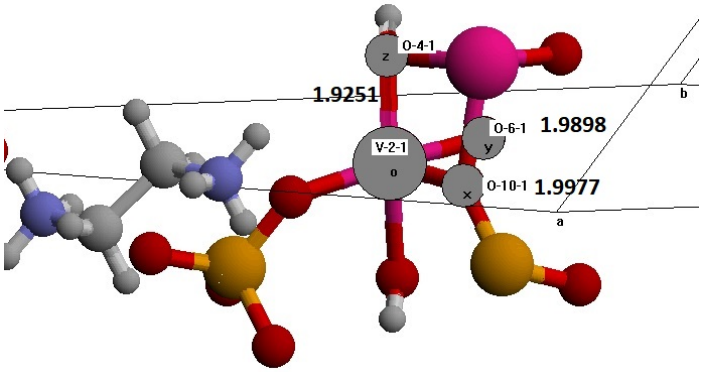

Figure S6. Local Cartesian coordinate system used for DFT+U+SOC calculations

(2) Computational parameters used

Exchange-correlation functional: PBE
Threshold for SCF convergence: 10^{-6} eV
k-point: (6x8x2) for $(enH_2)_{0.5}VPO_4OH$
(6x8x10) for NH_4VPO_4OH
Plane wave cut-off energy: 450 eV

(3) Results

Table S4. Relative energies ΔE (in K) of the ||z and ⊥z spin orientations of $(enH_2)_{0.5}VPO_4OH$ and NH_4VPO obtained from DFT+U+SOC calculations as well as the spin and orbital moments μ_S and μ_L (in μ_B).

For $(enH_2)_{0.5}VPO_4OH$

	U_{eff} = 3 eV		U_{eff} = 2 eV	
	//z	⊥z	//z	⊥z
ΔE	0	0.12	0	0.23
μ_S	1.890	1.890	1.874	1.874
μ_L	-0.019	-0.014	-0.023	-0.017

For NH_4VPO_4OH

	U_{eff} = 3 eV		U_{eff} = 2 eV	
	//z	⊥z	//z	⊥z
ΔE (K)	0	0.12	0)	0.12
μ_S	1.891	1.891	1.875	1.875
μ_L	-0.023	-0.018	-0.028	-0.023

C. Partial density of states (PDOS) plots for $(enH_2)_{0.5}VPO_4OH$ and NH_4VPO_4OH showing only the up-spin t_{2g} states

(a)

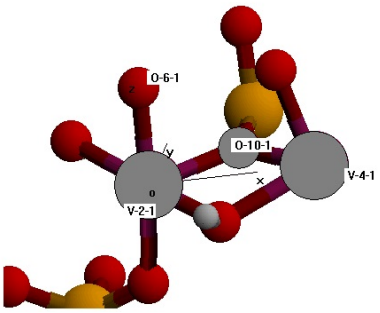

(b)

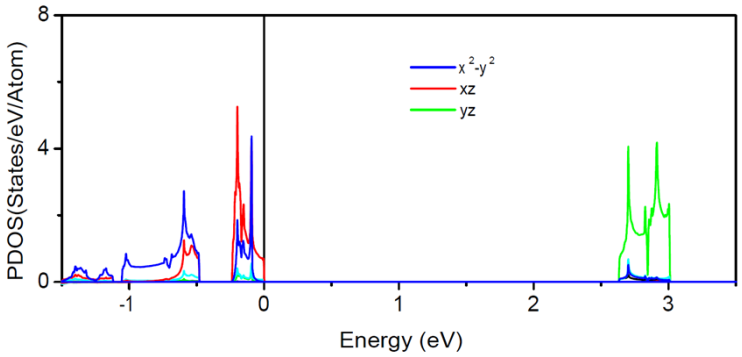

Figure S7. PDOS analysis for $(enH_2)_{0.5}VPO_4OH$: (a) The local Cartesian coordintes employed. (b) PDOS plots.

(a)

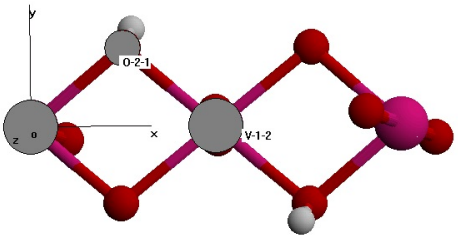

(b)

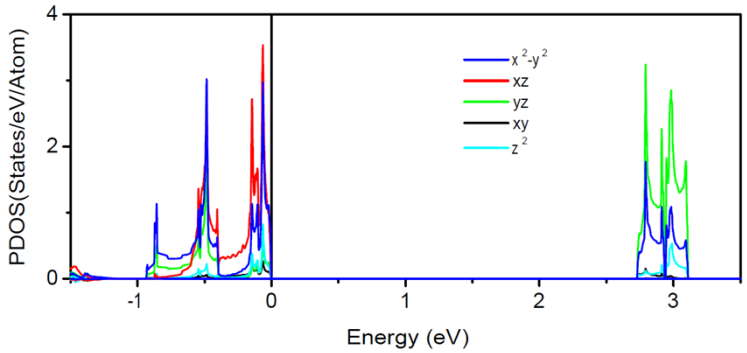

Figure S8. PDOS analysis for NH_4VPO_4OH: (a) The local Cartesian coordinates employed. (b) PDOS plots.

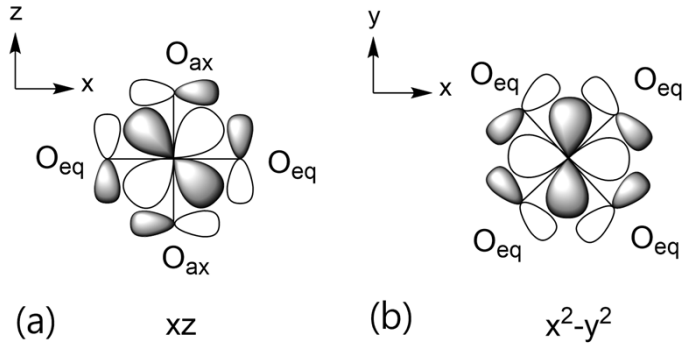

Figure S9. The p-orbitals of the O ligands that combine out-of-phase with the xz orbitals in (a), and with the x^2-y^2 orbitals in (b).

References

1. D. Fratzky, H. Worzala, Th. Goetze, M. Meisel, $NH_4VO(NH_3)PO_4$, *Acta Cryst. C* 1999, **55**, 156.
2. G. V. Kiriukhina, O. V. Yakubovich, O. V. Dimitrova, Crystal structure of a new polymorphic modification of niahite, $NH_4MnPO_4 \cdot H_2O$, *Crystallogr. Rep.* 2015, **60**, 198.
3. A. H. Liu, S. L. Wang, Novel Organically Templated Vanadyl(IV) Diarsenate and Monoarsenate with Chain Structures: Solvothermal Synthesis and Characterization of $(H_3NC_2H_4NH_3)[VO(H_2O)As_2O_7]$ and $(H_3NC_2H_4NH_3)_{0.5}[VO(H_2O)AsO_4]$, *Inorg. Chem.*, 1998, **37** (13), 3415.
4. T. Moriya, *Progress of Theoretical Physics* 1956, **16**, 23-44.
5. T. Shimizu, D.E. MacLaughlin, P.C. Hammel, J.D. Thompson, S.W. Cheong, Spin susceptibility and low-lying excitations in the Haldane-gap compound Y_2BaNiO_5, *Phys. Rev. B* 1995, **52**, R9835.
6. S. Capponi, M. Dupont, A.W. Sandvik, P. Sengupta, NMR relaxation in the spin-1 Heisenberg chain, *Phys. Rev. B* 2019, **100**, 094411.

7. K. Damle, S. Sachdev, Spin dynamics and transport in gapped one-dimensional Heisenberg antiferromagnets at nonzero temperatures, *Phys. Rev. B* 1998, **57**, 8307.
8. M. Takigawa, T. Asano, Y. Ajiro, M. Mekata, Y.J. Uemura, Dynamics in the S=1 One-Dimensional Antiferromagnet $AgVP_2S_6$ via ^{31}P and ^{51}V NMR, *Phys. Rev. Lett.* 1996, **76**, 2173.
9. B. Pedrini, J.L. Gavilano, D. Rau, H.R. Ott, S.M. Kazakov, J. Karpinski, S. Wessel, NMR and dc susceptibility studies of $NaVGe_2O_6$, *Phys. Rev. B* 2004, **70**(**2**), 024421.
10. T. Jolicur, O. Golinelli, σ-model study of Haldane-gap antiferromagnets, *Phys. Rev. B* 1994, **50**, 9265.
11. J. Sagi, & I. Affleck, Theory of nuclear magnetic relaxation in Haldane-gap antiferromagnets, *Phys. Rev. B* 1996, **53**, 9188.
12. B. Pahari, K. Ghoshray, R. Sarkar, B. Bandyopadhyay, A. Ghoshray, NMR study of 51V in quasi-one-dimensional integer spin chain compound $SrNi_2V_2O_8$, *Phys. Rev. B* 2006, **73**(**1**), 012407.
13. H. Xiang, C. Lee, H.-J. Koo, X. Gong, M.-H. Whangbo, Magnetic properties and energy-mapping analysis, *Dalton Trans.* 2013, **42**, 823.
14. M.-H. Whangbo, H. Xiang, *Magnetic Properties from the Perspectives of Electronic Hamiltonian*, Handbook of Solid State Chemistry. 2017.
15. M.-H. Whangbo, H.-J. Koo, R. K. Kremer, Spin Exchanges between Transition Metal Ions Governed by the Ligand p-Orbitals in Their Magnetic Orbitals, *Molecules* 2021, **26**, 531.
16. G. Kresse, D. Joubert, From ultrasoft pseudopotentials to the projector augmented-wave method, *Phys. Rev. B* 1999, **59**, 1758.
17. G. Kresse, J. Furthmüller, Efficient iterative schemes for *ab initio* total-energy calculations using a plane-wave basis set, *Comput. Mater. Sci.* 1996, **6**, 15.
18. J. P. Perdew, K. Burke, M. Ernzerhof, Generalized Gradient Approximation Made Simple, *Phys. Rev. Lett.* 1996, **77**, 3865.
19. S.L. Dudarev, G.A. Botton, S.Y. Savrasov, C.J. Humphreys, A.P. Sutton, Electron-energy-loss spectra and the structural stability of nickel oxide: An LSDA+U study, *Phys. Rev. B* 1998, **57**, 1505.
20. J. Kuneš, P. Novák, R. Schmid, P. Blaha, K. Schwarz, Electronic structure of fcc Th: Spin-orbit calculation with 6p1/2 local orbital extension, *Phys. Rev. B* 2001, **64**, 153102.